MPV17 encodes an inner mitochondrial membrane protein and is mutated in infantile hepatic mitochondrial DNA depletion

Antonella Spinazzola[1], Carlo Viscomi[1], Erika Fernandez-Vizarra[1], Franco Carrara[1], Pio D'Adamo[2], Sarah Calvo[3–5], René Massimiliano Marsano[6], Claudia Donnini[6], Hans Weiher[7], Pietro Strisciuglio[8], Rossella Parini[9], Emmanuelle Sarzi[10], Alicia Chan[11], Salvatore DiMauro[12], Agnes Rötig[10], Paolo Gasparini[2,13], Iliana Ferrero[6], Vamsi K Mootha[3–5], Valeria Tiranti[1] & Massimo Zeviani[1]

The mitochondrial (mt) DNA depletion syndromes (MDDS) are genetic disorders characterized by a severe, tissue-specific decrease of mtDNA copy number, leading to organ failure. There are two main clinical presentations: myopathic (OMIM 609560) and hepatocerebral[1] (OMIM 251880). Known mutant genes, including *TK2* (ref. 2), *SUCLA2* (ref. 3), *DGUOK* (ref. 4) and *POLG*[5,6], account for only a fraction of MDDS cases[7]. We found a new locus for hepatocerebral MDDS on chromosome 2p21-23 and prioritized the genes on this locus using a new integrative genomics strategy. One of the top-scoring candidates was the human ortholog of the mouse kidney disease gene *Mpv17* (ref. 8). We found disease-segregating mutations in three families with hepatocerebral MDDS and demonstrated that, contrary to the alleged peroxisomal localization of the *MPV17* gene product[9], MPV17 is a mitochondrial inner membrane protein, and its absence or malfunction causes oxidative phosphorylation (OXPHOS) failure and mtDNA depletion, not only in affected individuals but also in Mpv17^{−/−} mice.

We enrolled three families with MDDS (families 1–3; **Fig. 1a**) in this study. Individuals 1-1 and 1-3, originating from southern Italy, died of liver failure during the first year of life, but liver transplantation at 1 year of age in individual 1-2 and dietary control of hypoglycemia in individual 1-4 were effective in maintaining relative metabolic compensation and long-term survival. However, growth in the surviving children, who are 4 and 9 years old, has remained below the fifth

percentile, and the older child (individual 1-4) has developed neurological symptoms and multiple brain lesions documented by MRI (**Supplementary Fig. 1** online). Both probands 2-4 and 3-1 died in the first months after birth of liver failure; 2-4 was the fourth affected individual in a six-children sibship from first-cousin Moroccan parents; 3-1 was the second child of unrelated parents from Canada; her older brother is alive and well. We found marked mtDNA depletion in liver in all probands, associated with defects of mtDNA-related respiratory chain complexes (**Supplementary Fig. 1**). Normal or mildly reduced levels of mtDNA content and respiratory chain activities were found in muscle and cultured fibroblasts.

A genome-wide linkage analysis in family 1 gave a pairwise maximum lod score of 3.45 at $\Theta = 0$ with marker D2S390, and a maximum multipoint location score of 5.65 within a 19-cM region, between recombinant markers D2S2373 and D2S2259 on chromosome 2p21-23 (**Fig. 1b**). Haplotype reconstruction uncovered a homozygous condition caused by identity-by-descent alleles in the affected individuals (data not shown).

Because of the clinical and biochemical features of hepatocerebral MDDS, we assumed that the responsible protein was likely to be involved in mitochondrial metabolism and targeted to mitochondria. In order to prioritize candidate genes, we relied on a method, dubbed 'Maestro', that integrates eight different types of genomic data to make predictions about the human mitochondrial proteome and assign every gene a score of likelihood of localization to the mitochondrion[10]. Among the 151 genes annotated in the critical interval, Maestro spotlighted several previously unstudied high-scoring candidates as

[1]Unit of Molecular Neurogenetics, Pierfranco and Luisa Mariani Center for the Study of Children's Mitochondrial Disorders, National Neurological Institute "C. Besta", Milan 20126, Italy. [2]Linkage Unit & Service, Telethon Institute for Genetic Medicine (TIGEM), Naples 80131, Italy. [3]Center for Human Genetic Research, Massachusetts General Hospital, Cambridge, Massachusetts 02114, USA. [4]Department of Systems Biology, Harvard Medical School, Cambridge, Massachusetts, USA. [5]Broad Institute of the Massachusetts Institute of Technology and Harvard University, Cambridge 02446, Massachusetts, USA. [6]Department of Genetics Anthropology Evolution, University of Parma, Parma 43100, Italy. [7]University for Applied Sciences Bonn-Rhein-Sieg, Bonn, Germany 53359. [8]Department of Clinical and Experimental Medicine, University of Catanzaro Magna Graecia, Catanzaro 88100, Italy. [9]Unit of Pediatrics, Pierfranco and Luisa Mariani Center for the Study of Children's Metabolic Disorders, University Hospital, Milano-Bicocca State University, Monza 20052, Italy. [10]Department of Genetics and INSERM Unit U393, Hôpital Necker-Enfants Malades, Paris 75015, France. [11]Department of Medical Genetics, University of Alberta, Edmonton, Alberta, Canada T6G 2H7. [12]Department of Neurology, College of Physicians and Surgeons, Columbia University, New York, New York 10032, USA. [13]Department of Medical Genetics, University of Trieste, Trieste 34137, Italy. Correspondence should be addressed to M.Z. (zeviani@istituto-besta.it).
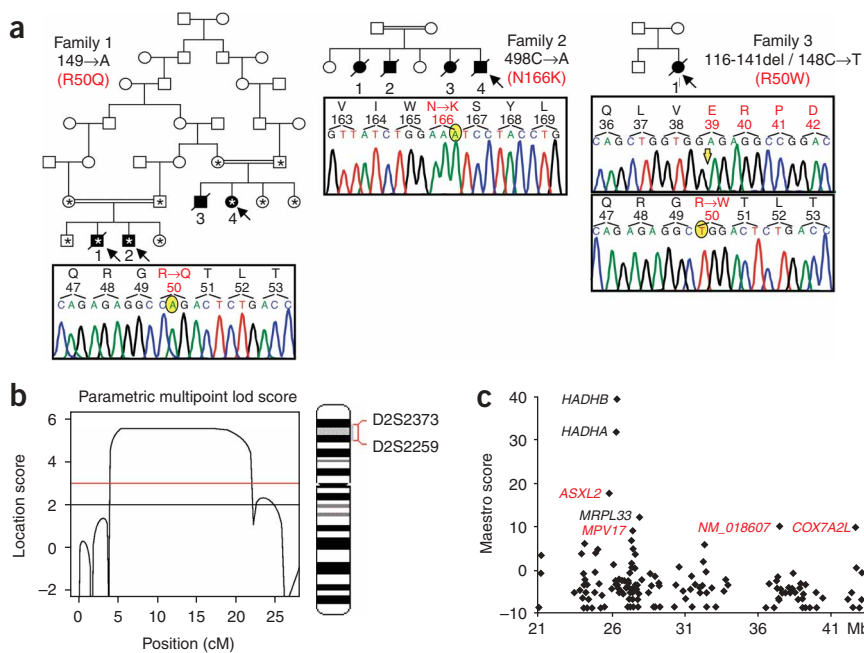
Figure 1 Linkage analysis, selection of candidate genes and mutation analysis. (**a**) Pedigrees. Filled symbols indicate affected individuals. Asterisks indicate the individuals of family 1 that participated in the genome-wide linkage analysis. Arrows indicate the probands. Beside each pedigree are the electropherograms of mutated *MPV17* sequences, with mutant nucleotides highlighted in yellow. Amino acid changes are indicated in red. Yellow arrow indicates the starting point of the 116–141 deletion in family 3. (**b**) Multipoint analysis of the hepatocerebral MDDS locus for family 1. An idiotype of chromosome 2 reports the position of the locus within the two flanking recombinant markers D2S2373 and D2S2259. (**c**) Prioritization of mitochondrial candidates within the D2S2373-D2S2259 linkage interval. For each gene (filled diamond) within the 19-Mb linkage peak, we plot the genomic position (*x*-axis) and the Maestro score (*y*-axis), which corresponds to the likelihood of encoding a mitochondrial protein. In addition to identifying the three known mitochondrial genes (black), this method identified four additional high-scoring candidates (red).

well as three genes already known to be mitochondrial (**Fig. 1c**). Sequencing of these genes (*HADHA*, *HADHAB* and *MRPL33*) and of *ASXL2*, *COX7A2L* and *NM_018607*, did not uncover any mutations segregating in the affected individuals. The seventh candidate was a ubiquitously expressed gene (**Fig. 2a**) annotated as the human ortholog of mouse *Mpv17* (ref. 8). We found a 149G→A (R50Q) homozygous mutation in the probands of family 1 and a 498C→A (N166K) homozygous mutation in the proband of family 2. The proband of family 3 was a compound heterozygote harboring a missense mutation in one allele (148C→T, R50W) and a 25-bp deletion in the other (116–141del; **Figs. 1a** and **2b**), which predicts the synthesis of an aberrant and prematurely truncated polypeptide. We found cosegregation of the mutations with the disease in all three families (data not shown). We did not detect any mutation in 500 samples from unrelated Italians and 30 from unrelated Arabs.

The three missense mutations affected amino acid residues conserved from the facultative aerobic yeast *Saccharomyces cerevisiae* (**Fig. 2c**), in which the *MPV17* ortholog is known as *SYM1* (ref. 11), to humans. To validate the pathogenic significance of the human mutations, we used a *SYM1*-defective yeast strain (*Δsym1*), which fails to grow at 37 °C in medium containing ≥2% ethanol[11] as the only carbon source. This temperature-sensitive OXPHOS phenotype is rescued by reexpressing the wild-type *SYM1* gene, or, albeit less effectively, the mammalian *MPV17* gene[11] (**Fig. 3a**). We obtained very limited correction by reexpressing *sym1*[R51Q], a variant harboring the mutation equivalent to human R50Q, but we did not obtain any correction with *sym1*[R51W] and *sym1*[N172K], equivalent to human R50W and N166K. None of the human *MPV17* mutant variants were able to rescue the *Δsym1* phenotype (**Fig. 3a**). These results indicate that the human *MPV17* mutations are deleterious in yeast. The *sym1*[R51Q] had less drastic effects, as does the R50Q in humans, which seems to cause a relatively milder phenotype. mtDNA instability in *S. cerevisiae* is associated with increased segregation of respiratory-deficient 'petite' mutants[12]. When the *Δsym1* strains reexpressing the mutant *SYM1* variants were grown on ethanol- and glucose-containing medium at 37 °C, they produced a significant increase of respiratory-deficient mutants, suggesting a role for *SYM1* in maintaining mtDNA integrity

and stability (**Fig. 3b**). To evaluate the nature of the petite mutations (ρ^- versus ρ^0), we used a DNA blot to analyze the mtDNA of *sym1*[R51Q], *sym1*[R51W] and *sym1*[N172K] respiratory-deficient clones. Rearranged mtDNA was present in all three (**Fig. 3c**), indicating that the pathological alleles induced ρ^- mutations.

The *SYM1* gene product (Sym1p) has recently been shown to target, and reside in, the yeast inner mitochondrial membrane (IMM)[11]. Likewise, a high score for potential mitochondrial targeting was given to the MPV17 N terminus by *ad hoc* algorithms, including Maestro (see above). To test experimentally the hypothesis that mammalian MPV17 is also a mitochondrial protein, we first transfected a construct
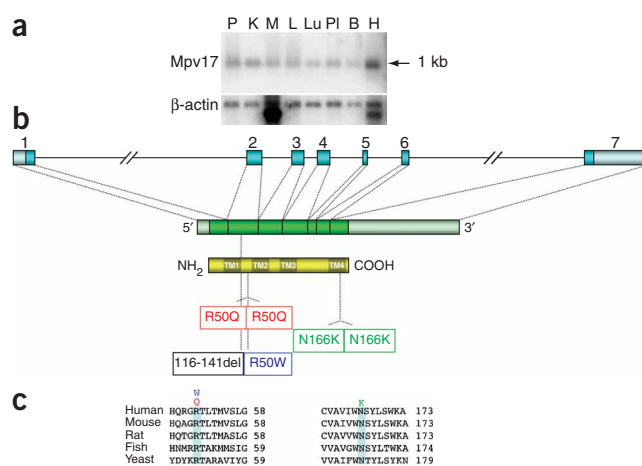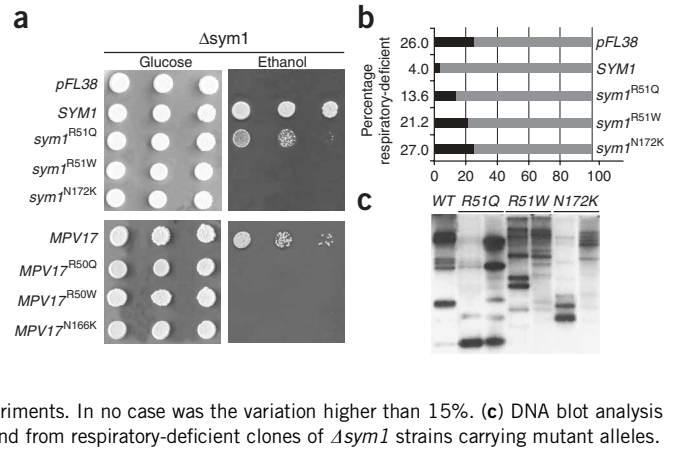

Figure 2 *MPV17* transcript, gene organization and protein. (**a**) RNA blot analysis on polyA(+) RNA extracted from human pancreas (P), kidney (K), muscle (M), liver (L), lung (Lu), placenta (Pl), brain (B) and heart (H). (**b**) Schematic representation of the seven exons of the *MPV17* gene, transcript and protein, showing mutations found in our families. Darker hues indicate the ORF sequences; lighter hues indicate the 5′ and 3′ UTRs. (**c**) CLUSTALW multiple alignments of the MPV17 regions containing the amino acids mutated in our families. Amino acid substitutions are shown in color above the alignments.

Figure 3 Complementation studies in *Saccharomyces cerevisiae*. (**a**) Oxidative growth phenotype at 37 °C. The BY4741 *Δsym1* mutant was transformed with either empty pFL38, pFL38 carrying *SYM1*, pFL38 carrying the pathological (*sym1*R51Q, *sym1*R51W and *sym1*N172K) alleles, pYEX carrying the human wild-type human allele (*MPV17*), or pYEX carrying mutant human alleles (*MPV17*R50Q, *MPV17*R50W and *MPV17*N166K) alleles. Equal amounts of serial dilutions of cells from exponentially grown cultures (10^5, 10^4 and 10^3 cells) were spotted onto YNB plates supplemented with 2% glucose or YP plates supplemented with 2% ethanol. Growth was scored after 5 d of incubation at 37 °C. (**b**) Respiratory-deficient mutant accumulation in *Δsym1* strains carrying mutant alleles. Black bars and gray bars represent the percentage of respiratory-deficient and respiratory-competent colonies, respectively. The percentage of the respiratory-deficient colonies is shown at left for each recombinant strain. The diagnosis of respiratory-deficient (petite) mutants was carried out on YNB plates supplemented with 0.2% glucose and 2% ethanol. More than 1,000 colonies per strain were scored. All values are means of three independent experiments. In no case was the variation higher than 15%. (**c**) DNA blot analysis showing the mtDNA patterns obtained from the parental wild-type (WT) strain and from respiratory-deficient clones of *Δsym1* strains carrying mutant alleles.
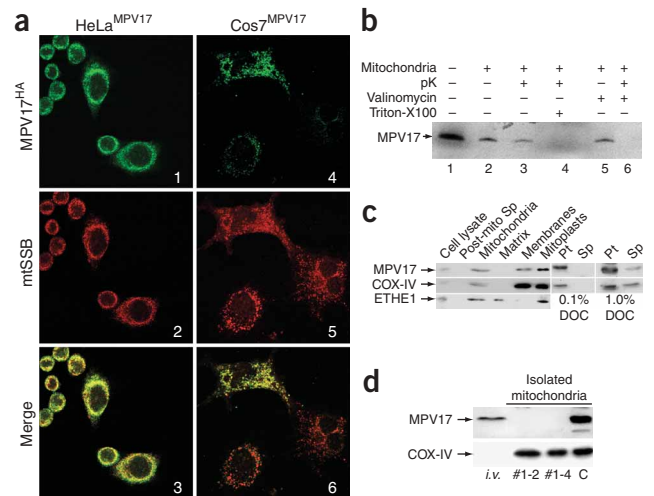
expressing MPV17HA, a recombinant human MPV17 tagged on the C terminus with the hemagglutinin (HA) epitope of the influenza virus. Transient and stable transfections were performed in COS7 and HeLa cells, respectively. In both cell systems, the immunofluorescence pattern specific to MPV17HA coincided with that of the mitochondrial single-stranded DNA binding protein[13] (**Fig. 4a**) or MitoTracker, a mitochondrion-specific dye (data not shown).

To demonstrate active mitochondrial import, we incubated radiolabeled *in vitro*–translated MPV17 with freshly prepared, energized HeLa cell mitochondria (**Fig. 4b**). Treatment with proteinase K did not digest this translation product in intact mitochondria but completely digested it after solubilization of mitochondrial membranes with Triton X-100, indicating that the polypeptide was located inside the organelle. The import process was dependent on the mitochondrial protonmotive force (ΔΨ), as we obtained complete proteinase K digestion after treatment with valinomycin, an ionophore that abolishes ΔΨ. These results demonstrate that MPV17 is imported into mitochondria through the ΔΨ-dependent TOM-TIM import machinery[14,15], which targets proteins to either the IMM or the mitochondrial matrix. Notably, the *MPV17*-specific *in vitro* translation product had the

same electrophoretic mobility before and after internalization into mitochondria (**Fig. 4b**). This result indicates that MPV17 is not cleaved after the import process is completed, contrary to what is usually seen for most IMM or mitochondrial matrix proteins. These proteins contain an N-terminal presequence that is cleaved by the mitochondrial processing peptidase[16] after mitochondrial internalization through the TIM23 complex[14]. The absence of post-import cleavage is typical of IMM carrier proteins, which are inserted into the IMM by the TIM22 complex[14,15,17], but it has also been documented for a few other IMM or mitochondrial matrix proteins[18,19].

To clarify which mitochondrial compartment MPV17 belongs to, we performed a series of protein blot experiments on different cellular and suborganellar fractions, using an antibody to MPV17. We detected material cross-reacting with MPV17 (CRM) in intact HeLa cell mitochondria (**Fig. 4c**; same preparation as in **Fig. 4b**). We detected enrichment of MPV17 CRM in both the mitochondrial membrane fraction and in mitoplasts (that is, organelles in which the outer mitochondrial membrane was disrupted and the content of the intermembrane space (IMS) was washed out). We did not detect any MPV17 CRM in the mitochondrial matrix (**Fig. 4c**).

Figure 4 Mitochondrial localization of MPV17. (**a**) Confocal immunofluorescence on stably transfected HeLaMPV17 cells and transiently transfected Cos7MPV17 cells. mtSSB, mitochondrial single-stranded DNA binding protein. The two immunofluorescence patterns overlap (bottom row). Magnification, 40×. (**b**) *In vitro* mitochondrial import of human MPV17, as shown by ^{35}S autoradiography. Lane 1: MPV17 (translated *in vitro*); 2: MPV17 (translated *in vitro*) after exposure to intact, energized mitochondria; 3: MPV17 is protected from proteinase K (pK) digestion; 4: MPV17 is completely digested by pK after solubilization of mitochondria with Triton X-100; 5: valinomycin abolishes mitochondrial ΔΨ; 6: mitochondrial import is abolished, as demonstrated by complete pK digestion of the protein. (**c**) Suborganellar localization of MPV17, as shown by protein blot analysis on mitochondria isolated from HeLa cells. MPV17 CRM is present in the HeLa cell lysate but is absent in the postmitochondrial supernatant (Sp) and the mitochondrial matrix. Progressive enrichment of MPV17 CRM is evident in isolated mitochondria, mitochondrial membranes and digitonin-treated mitochondria (mitoplasts). Treatment of mitochondrial membranes with 0.1% deoxycholate (DOC) did not release MPV17 from the pellet (Pt) to the supernatant; very limited release was obtained using 1% DOC. Overlapping results were obtained using an antibody against COX-IV, a known component of the mitochondrial inner membrane. By contrast, the CRM for ETHE1 is localized in the mitochondrial matrix[12]. (**d**) Protein blot analysis of MPV17 on mitochondria isolated from fibroblasts of individuals 1-2 and 1-4 and of an age-matched control individual (C). The specificity of the antibody to MPV17 was demonstrated by immunostaining of human *in vitro* (*i.v.*)-translated MPV17.
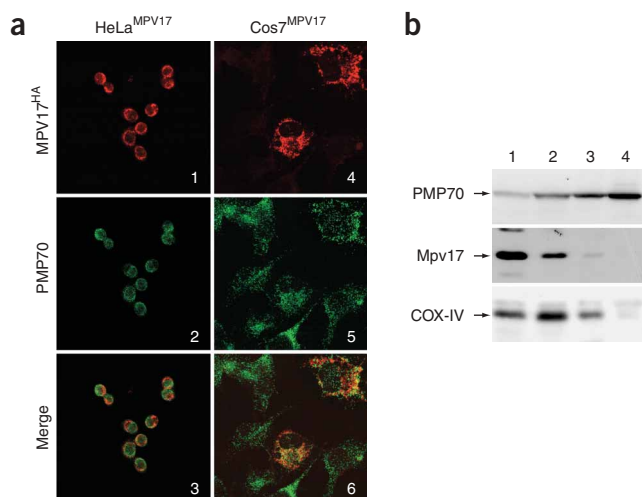
a

b

Figure 5 Mpv17 versus peroxisomal PMP70 immunostaining. (**a**) Confocal immunofluorescence on stably transfected HeLa[MPV17] cells and transiently transfected Cos7[MPV17] cells. The two immunofluorescence patterns do not overlap (bottom row). Magnification, 40×. (**b**) Protein blot analysis of different cell fractions from mouse liver, including a 2,000g fraction containing 'heavy' mitochondria (lane 1), a 25,000g fraction enriched in peroxisomes and 'light' mitochondria (lane 2), and two 100,000g iodixanol gradient fractions separating 'light' mitochondria and microsomes (lane 3) from purified peroxisomes (lane 4). Enrichment in the content of peroxisomes can be seen in the increasing intensity of the PMP70-specific band from left to right. No mitochondrial contamination is present in the purified peroxisomal fraction (lane 4), as demonstrated by the virtual absence of COX-IV CRM.

Treatment of the mitochondrial membrane fraction with increasing concentrations of deoxycholate (**Fig. 4c**) or with 0.1 M Na$_2$CO$_3$ (**Supplementary Fig. 2** online), demonstrated that MPV17 is a tightly bound membrane protein. Taken together, these experiments indicate that MPV17 is an IMM protein. This conclusion is further supported by the four hydrophobic, potential transmembrane domains found in Sym1p (ref. 11), which are conserved in MPV17 (**Fig. 2b**). Finally, we did not find any MPV17 CRM in mitochondria isolated from fibroblasts of individuals 1-2 and 1-4 (**Fig. 4d**), suggesting that the R50Q mutation causes protein instability and decay.
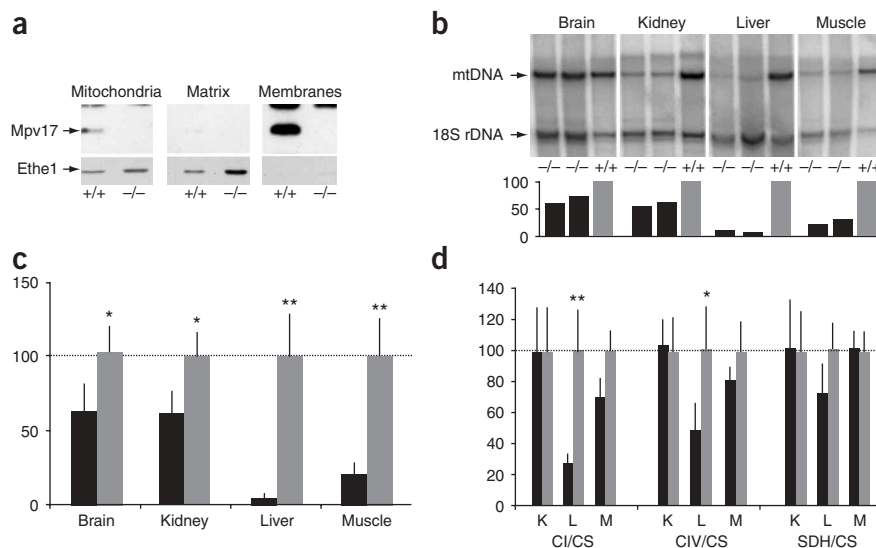
In contrast with previous studies that suggested that Mpv17 was localized in the membrane of peroxisomes[9], our MPV17[HA] immuno-fluorescence pattern consistently failed to match the pattern specific to the peroxisomal membrane protein PMP70 (**Fig. 5a**). These results, and those obtained by protein blot analysis on mouse liver mitochondria and purified peroxisomes (**Fig. 5b**), clearly demonstrate that MPV17 is largely, if not exclusively, confined to mitochondria.

The *Mpv17* gene was first identified as the target of a transgene insertion by a retroviral genome in a mouse germinal line, resulting in *Mpv17*^{−/−} animals[9]. Accordingly, we did not find any Mpv17 CRM in mitochondria isolated from *Mpv17*^{−/−} livers (**Fig. 6**). The mtDNA content, measured by real-time PCR (**Fig. 6**), was markedly decreased in liver of *Mpv17*^{−/−} mice (approximately 4% ± 3 s.d. of mean control values) and progressively less so in muscle (20% ± 8%), kidney (60% ± 19%) and brain (60% ± 18%). We obtained similar results by DNA blot analysis (**Fig. 6b**). MtDNA-dependent respiratory chain activities (complex I and complex IV) were consistently and significantly decreased in liver of *Mpv17*^{−/−} animals but were normal in muscle and kidney (**Fig. 6d**).

The *Mpv17*^{−/−} mice have been reported to develop age-dependent hearing loss[20] and severe renal failure owing to glomerular sclerosis[8]. However, after these initial observations, the kidney disease could no longer be documented in *Mpv17*^{−/−} mouse strains investigated at different ages and in different research centers (M.Z., personal observation). We are baffled by the disappearance of this phenotype. A possible explanation is genetic selection of adaptive mechanisms that markedly reduced the penetrance of the kidney-specific trait. A less likely explanation is that this trait was due to a second mutation in another gene that was lost over time during the selection of *Mpv17*^{−/−} and *Mpv17*^{+/−} individuals.

Figure 6 Characterization of *Mpv17*^{−/−} mice. (**a**) Protein blot analysis of Mpv17 on liver mitochondria and submitochondrial fractions of 6-month-old *Mpv17*^{−/−} and age-matched *Mpv17*^{+/+} control mice. Five animals were used for each series. No Mpv17-CRM was detected in the *Mpv17*^{−/−} samples. (**b**) DNA blot analysis of linearized mtDNA extracted from different tissues of two *Mpv17*^{−/−} mice versus one *Mpv17*^{+/+} mouse. The band corresponding to 18S ribosomal DNA (rDNA) serves as a standard index of the nuclear DNA content in each sample. Histogram below the DNA blot shows the mtDNA/18S rDNA ratios measured densitometrically in the *Mpv17*^{−/−} mice (black) and *Mpv17*^{+/+} mouse (gray), normalized to 100%. (**c**) Real-time PCR quantification of the amount of mtDNA relative to that of GAPDH, a nuclear gene used as a standard. Five *Mpv17*^{−/−} mice (black) were compared with five age-matched *Mpv17*^{+/+} mice (gray), normalized to 100%. **, $P < 0.001$; *, $P < 0.01$ (two-tailed unpaired Student's *t*-test). (**d**) Specific activities of complex I (CI), complex IV (CIV) and succinate dehydrogenase (SDH), normalized to the specific activity of citrate synthase (CS), in kidney (K), liver (L), and muscle (M) homogenates from five *Mpv17*^{−/−} mice (black) and five age-matched *Mpv17*^{+/+} mice (gray), normalized to 100%. SDH is a respiratory chain complex that is encoded entirely in the nucleus. **, $P < 0.001$; *, $P < 0.01$ (two-tailed unpaired Student's *t*-test).

Contrary to observations in humans, the absence of Mpv17 is compatible with survival to adulthood in *Mpv17*^{−/−} mice. However, in the affected individuals used in this study, metabolic failure occurs, or worsens substantially, during stress challenges such as fasting or febrile episodes, conditions that are not experienced by laboratory animals. Further studies, including stress challenges, are warranted to assess the mitochondrial pathophysiology of *Mpv17*^{−/−} mice.

The temperature-sensitive phenotype of the *Δsym1* yeast strain suggests a role for Sym1p in the cellular response to stress[11]. In mouse fibroblasts, the absence of Mpv17 reduces, and its overexpression increases, the production of reactive oxygen species[9]. In addition, our own findings indicate a role for MPV17 in controlling mtDNA maintenance and OXPHOS activity in mammals and yeast. Taken together, these results provide clues for future studies of the function of this protein in mitochondrial homeostasis.

METHODS

Patients and DNA samples. All procedures were approved by the Review Board of the National Neurological Institute 'C. Besta'. We obtained informed consent from parents of all probands and siblings before collecting blood for DNA extraction or performing tissue biopsies. The treatment of animals was according to the corresponding guidelines approved by the Ethical Committee of the National Neurological Institute, Italy.

Linkage analysis. A genome-wide search was performed using the Applied Biosystems (ABI) PRISM Linkage Mapping Set v. 2.5 on an ABI PRISM 3100 DNA sequencer, and results were processed by GENESCAN software. Alleles were assigned using the GENOTYPER software. Statistical analysis was performed assuming complete penetrance of a recessive disease. Pairwise linkage analysis and multipoint analysis were performed using the LINKAGE computer package and Simwalk2, respectively.

Identification of mitochondrial candidates. Every gene in the linkage region (D2S2373–D2S2259), based on Ensembl annotations, was assigned a Maestro score representing the likelihood of mitochondrial localization. The likelihood scores were computed based on a naive Bayesian integration of eight genomic data sets, where the contribution of each data set was weighted by its accuracy. A significance threshold was determined based on a large training set of known mitochondrial proteins.

Antibodies. The affinity-purified polyclonal antibody to Mpv17 was from Proteintech, and the polyclonal antibody specific to the peroxisomal membrane marker PMP70 was from Sigma. The mouse monoclonal antibody to the hemagglutinin epitope of the influenza virus (anti-HA) was from Roche; the monoclonal antibody against cytochrome *c* oxidase subunit IV was from Molecular Probes/Invitrogen. Polyclonal antibodies against human mitochondrial single-stranded DNA binding protein and ETHE1 were raised in rabbit and characterized as described[13]. Cross-reactivity of the antibody to Mpv17 was confirmed by immunostaining of a human MPV17 recombinant protein obtained by *in vitro* translation (see **Fig. 4d**).

Cell cultures and immunofluorescence studies. Mammalian cells were cultured in DMEM + 10% fetal calf serum (FCS) at 37 °C in a 5% CO_2 atmosphere. For immunofluorescence analysis, cells were plated on coverslips, followed by fixation and incubation with primary and fluorescent dye–conjugated secondary antibodies, as described[13]. In some experiments, cells were preincubated with 100 nM MitoTracker Red dye (Molecular Probes) for 45 min at 37 °C. Fluorescence patterns were visualized by a confocal microscope (BioRad).

Protein blot analysis. Approximately 2×10^7 cells were used to prepare mitochondrial fractions in both HeLa cells and human fibroblasts[21]. Equal amounts of non-collagen protein (50–100 µg protein per lane) were used in SDS-polyacrylamide gel electrophoresis and protein blot analysis, as described[13].

Cell fractionation. Standard methods were used for the preparation of cell lysates, mitochondrial and postmitochondrial fractions in cultured cells and tissue homogenates[21]. For suborganellar localization, freshly isolated mitochondria from HeLa cells were treated with three cycles of freezing-thawing and six sonication strokes at 4 °C. The membrane and soluble fractions were then separated by ultracentrifugation at $10^5 g$ for 1 h at 4 °C. Mitoplasts were isolated from mitochondria from HeLa cells by either digitonin treatment[22] or hypoosmotic shock[23]. In some experiments, mitochondrial membranes were treated with the nonionic detergent deoxycholate[24] or with 0.1 M Na_2CO_3, pH 11.0 (ref. 25). Isolation of peroxisomes from mouse liver based on iodixanol gradient centrifugation was performed using the Peroxisome Isolation Kit (Sigma).

Biochemical assays. Specific activities of individual respiratory chain complexes were measured on cell and tissue homogenates[26]. Specific activities of each complex were normalized to that of citrate synthase (CS)[26], an indicator of the number of mitochondria.

In vitro import assay. A human *MPV17* cDNA was amplified by PCR using suitable pairs of primers flanking the coding region. The T7 phage promoter was incorporated in the sense primer for *in vitro* transcription of the PCR fragment. *In vitro* transcription and translation were performed using the TNT T7 Quick Coupled Transcription/Translation System (Promega) in the presence of 20 µCi [35S]methionine (Amersham). Fresh mitochondria were prepared from 2×10^7 HeLa cells[21] and were resuspended with incubation buffer[27] to a final protein concentration of 2 mg ml⁻¹. The *in vitro* import assay was then carried out as described[27]. Samples were resuspended in 20 µl solubilization buffer[24], boiled for 5 min and separated on a 16% SDS-polyacrylamide gel. After fixation in 10% acetic acid/25% isopropanol, the gel was washed for 20 min in Amplify reagent (Amersham) and exposed using a phosphorimaging screen (Biorad).

Generation of human MPV17 mutant variants. The QuikChange Site-Directed Mutagenesis Kit (Stratagene) and the oligonucleotide pairs reported in **Supplementary Table 1** online were used to introduce three different point mutations in the human *MPV17* cDNA. After mutagenesis, sequences of inserts were verified on both strands.

Yeast strains and culture media. Yeast strains were BY4741 (*MAT*α *his3*Δ1 *leu2*Δ0 *lys2*Δ0 *ura3*Δ0) and its isogenic *Δsym1::kanMX4* mutant. Cells were cultured in 0.67% Yeast Nitrogen Base (YNB) medium without amino acids (Difco), supplemented with the appropriate amino acids and bases to a final concentration of 40 µg ml⁻¹. Various carbon sources were added at 2% (wt/vol).

The *SYM1* gene was amplified by PCR from the BY4741 wild-type strain and cloned into the centromeric yeast plasmid pFL38. Site-directed mutagenesis, performed by the overlap extension technique[28], was used to introduce three different point mutations in the *S. cerevisiae SYM1* gene. The list of base changes and corresponding modified primers used to generate mutated alleles are listed in **Supplementary Table 1**. Sequences of mutant inserts were verified on both strands. Both wild-type and mutated human *MPV17* cDNAs were cloned into the pYEX plasmid. The *Δsym1* strain was transformed as previously described[29].

For respiratory-deficient diagnosis (petite colonies), cells from cultures grown for seven generations in YNB supplemented with glucose and ethanol at 37 °C were plated onto solid YNB medium containing 2% ethanol and 0.2% glucose and maintained for 5 d at 28 °C. PCR-based analysis of mtDNA on respiratory-deficient colonies was performed as previously described[28].

Generation and cloning of MPV17[HA]. A full-length human *MPV17* cDNA clone was obtained from the RZPD consortium (clone IRAUp969G055D6). A chimeric oligonucleotide primer containing the 3′ end of the human *MPV17* cDNA ORF in frame with HA encoding sequence[13] was used to obtain an HA-tagged *MPV17* cDNA fragment that was inserted into the eukaryotic expression plasmid vector pcDNA3.1 (Invitrogen) using suitable restriction sites. The recombinant plasmid was transfected by electroporation in Cos7 (for transient expression) or in HeLa (for stable expression) cells as previously described[13].

DNA blot and real-time PCR. Total DNA was extracted from human liver and muscle biopsies and from different mouse tissues, following standard procedures. For DNA blot analysis, mouse and human mtDNAs were linearized using the restriction enzymes *Sac*I and *Pvu*II, respectively. Species-specific 1-kb probes encompassing the human or mouse mtDNA sequence encoding cytochrome *c* oxidase subunit I (COI) were used for mtDNA detection. A 1-kb probe encompassing part of the sequence encoding the mouse nuclear 18S rDNA (**Supplementary Table 2** online) was used as a standard index of the nuclear DNA content in each sample for densitometric measurements. Both probes were labeled with ^{32}P using the Decaprime II kit (Ambion). Yeast mtDNA was extracted by rapid mitochondrial preparation, digested with *Eco*RV (Amersham) and detected by DNA blot analysis, as described[28].

Real-time quantitative PCR on mouse mtDNA was carried out using an ABI PRISM 7000 Sequence Detection System in a two-step reaction, essentially as described previously[30]. Primers and detection probe specific to a region of the murine COI gene were designed using ABI Primer Express software (**Supplementary Table 2**). Each PCR reaction was performed in triplicate with the following profile: one cycle at 50 °C for 2 min, one cycle at 95 °C for 10 min, and then 40 cycles of 95 °C for 15 s and 60 °C for 1 min (two-step protocol). Primers and detection probe of the genes encoding either human RNase-P or mouse glyceraldehyde-3-phosphate dehydrogenase were used as nuclear gene standard references, according the instructions of the manufacturer.

RNA blot. A pre-made multiple-tissue RNA blot containing 1 µg per lane of purified polyA(+) RNA (Clontech) was incubated in ExpressHyb Hybridization Solution (Clontech) for 30 min at 65 °C and then was hybridized for 2 h at 65 °C with a ^{32}P-labeled human *MPV17* cDNA (Decaprime II, Ambion). The multiple-tissue RNA blot filter was exposed overnight and visualized by a phosphorimager apparatus (BioRad).

Genotyping. Nucleotide sequence analysis was carried out on a 3100 ABI Automated Sequencer on samples prepared using the BigDye Termination kit (Applied Biosystems). Data were elaborated using Secscape software (Applied Biosystems). The oligonucleotide primers used for PCR amplification of the seven exons of the human *MPV17* gene are listed in **Supplementary Table 3** online. PCR amplification conditions for exon 1, exons 4–6 and exon 7 were an initial denaturation step at 94 °C for 3 min; followed by 32 cycles of 94 °C for 1 min, 54 °C for 30 s and 72 °C for 1 min; plus a final extension at 72 °C for 2 min. Exon 2 and exons 3+4 were amplified as above, except that the annealing temperature was 58 °C.

Statistics. A two-tailed, unpaired Student's *t*-test was used to calculate the significance of biochemical and molecular data.

URLs. NCBI-Unigene: http://www.ncbi.nlm.nih.gov; Mitoprot2: http://mips.gsf.de/cgi-bin/proj/medgen/mitofilter; PSORT: http://psort.nibb.ac.jp/; Predotar: http://www.inra.fr/predotar/french.html; TargetP: http://www.cbs.dtu.dk/services/TargetP/; CLUSTALW: http://www.ebi.ac.uk/clustalw/; rzpd: http://www.rzpd.de/; Ensembl: http://www.ensembl.org.

Note: Supplementary information is available on the Nature Genetics website.

1. Spinazzola, A. & Zeviani, M. Disorders of nuclear-mitochondrial intergenomic signaling. *Gene* **354**, 162–168 (2005).
2. Saada, A. *et al.* Mutant mitochondrial thymidine kinase in mitochondrial DNA depletion myopathy. *Nat. Genet.* **29**, 342–344 (2001).
3. Elpeleg, O. *et al.* Deficiency of the ADP-forming succinyl-CoA synthase activity is associated with encephalomyopathy and mitochondrial DNA depletion. *Am. J. Hum. Genet.* **76**, 1081–1086 (2005).
4. Mandel, H. *et al.* The deoxyguanosine kinase gene is mutated in individuals with depleted hepatocerebral mitochondrial DNA. *Nat. Genet.* **29**, 337–341 (2001).
5. Nguyen, K.V. *et al.* POLG mutations in Alpers syndrome. *Neurology* **65**, 1493–1495 (2005).
6. Ferrari, G. *et al.* Infantile hepatocerebral syndromes associated with mutations in the mitochondrial DNA polymerase-gammaA. *Brain* **128**, 723–731 (2005).
7. Salviati, L. *et al.* Mitochondrial DNA depletion and dGK gene mutations. *Ann. Neurol.* **52**, 311–317 (2002).
8. Weiher, H., Noda, T., Gray, D.A., Sharpe, A.H. & Jaenisch, R. Transgenic mouse model of kidney disease: insertional inactivation of ubiquitously expressed gene leads to nephrotic syndrome. *Cell* **62**, 425–434 (1990).
9. Zwacka, R.M. *et al.* The glomerulosclerosis gene Mpv17 encodes a peroxisomal protein producing reactive oxygen species. *EMBO J.* **13**, 5129–5134 (1994).
10. Calvo, S. *et al.* Systematic identification of human mitochondrial disease genes through integrative genomics. *Nat. Genet.*, advance online publication 2 April 2006 (doi:10.1038/ng1776).
11. Trott, A. & Morano, K.A. SYM1 is the stress-induced *Saccharomyces cerevisiae* ortholog of the mammalian kidney disease gene Mpv17 and is required for ethanol metabolism and tolerance during heat shock. *Eukaryot. Cell* **3**, 620–631 (2004).
12. Mounolou, J.C., Jakob, H. & Slonimski, P.P. Mitochondrial DNA from yeast "petite" mutants: specific changes in buoyant density corresponding to different cytoplasmic mutations. *Biochem. Biophys. Res. Commun.* **24**, 218–224 (1966).
13. Tiranti, V. *et al.* Ethylmalonic encephalopathy is caused by mutations in ETHE1, a gene encoding a mitochondrial matrix protein. *Am. J. Hum. Genet.* **74**, 239–252 (2004).
14. Koehler, C.M. New developments in mitochondrial assembly. *Annu. Rev. Cell Dev. Biol.* **20**, 309–335 (2004).
15. Wiedemann, N., Frazier, A.E. & Pfanner, N. The protein import machinery of mitochondria. *J. Biol. Chem.* **279**, 14473–14478 (2004).
16. Gakh, O., Cavadini, P. & Isaya, G. Mitochondrial processing peptidases. *Biochim. Biophys. Acta* **1592**, 63–77 (2002).
17. Rehling, P., Pfanner, N. & Meisinger, C. Insertion of hydrophobic membrane proteins into the inner mitochondrial membrane – a guided tour. *J. Mol. Biol.* **326**, 639–657 (2003).
18. Otsuka, M., Mizuno, Y., Yoshida, M., Kagawa, Y. & Ohta, S. Nucleotide sequence of cDNA encoding human cytochrome c oxidase subunit VIc. *Nucleic Acids Res.* **16**, 10916 (1988).
19. Hammen, P.K., Gorenstein, D.G. & Weiner, H. Structure of the signal sequences for two mitochondrial matrix proteins that are not proteolytically processed upon import. *Biochemistry* **33**, 8610–8617 (1994).
20. Meyer zum Gottesberge, A.M., Reuter, A. & Weiher, H. Inner ear defect similar to Alport's syndrome in the glomerulosclerosis mouse model Mpv17. *Eur. Arch. Otorhinolaryngol.* **253**, 470–474 (1996).
21. Fernandez-Vizarra, E., Lopez-Perez, M.J. & Enriquez, J.A. Isolation of biogenetically competent mitochondria from mammalian tissues and cultured cells. *Methods* **26**, 292–297 (2002).
22. Gallet, P.F. *et al.* Transbilayer movement and distribution of spin-labelled phospholipids in the inner mitochondrial membrane. *Biochim. Biophys. Acta* **1418**, 61–70 (1999).
23. Ohba, M. & Schatz, G. Disruption of the outer membrane restores protein import to trypsin-treated yeast mitochondria. *EMBO J.* **6**, 2117–2122 (1987).
24. Tiranti, V. *et al.* Characterization of SURF-1 expression and Surf-1p function in normal and disease conditions. *Hum. Mol. Genet.* **8**, 2533–2540 (1999).
25. Fujiki, Y., Hubbard, A.L., Fowler, S. & Lazarow, P.B. Isolation of intracellular membranes by means of sodium carbonate treatment: application to endoplasmic reticulum. *J. Cell. Biol.* **93**, 97–102 (1982).
26. Bugiani, M. *et al.* Clinical and molecular findings in children with complex I deficiency. *Biochim. Biophys. Acta* **1659**, 136–147 (2004).
27. Petruzzella, V. *et al.* Identification and characterization of human cDNAs specific to BCS1, PET112, SCO1, COX15, and COX11, five genes involved in the formation and function of the mitochondrial respiratory chain. *Genomics* **54**, 494–504 (1998).
28. Ho, S.N., Hunt, H.D., Horton, R.M., Pullen, J.K. & Pease, L.R. Site-directed mutagenesis by overlap extension using the polymerase chain reaction. *Gene* **77**, 51–59 (1989).
29. Fontanesi, F. *et al.* Mutations in AAC2, equivalent to human adPEO-associated ANT1 mutations, lead to defective oxidative phosphorylation in *Saccharomyces cerevisiae* and affect mitochondrial DNA stability. *Hum. Mol. Genet.* **13**, 923–934 (2004).
30. Winterthun, S. *et al.* Autosomal recessive mitochondrial ataxic syndrome due to mitochondrial polymerase gamma mutations. *Neurology* **64**, 1204–1208 (2005).